

Microscopic description of fission in neutron-rich Radium isotopes with the Gogny energy density functional

R. Rodríguez-Guzmán¹ and L. M. Robledo²

¹ *Physics Department, Kuwait University, Kuwait 13060, Kuwait.*

² *Departamento de Física Teórica, Universidad Autónoma de Madrid, 28049-Madrid, Spain*

(Dated: October 7, 2015)

Mean field calculations, based on the D1S, D1N and D1M parametrizations of the Gogny energy density functional, have been carried out to obtain the potential energy surfaces relevant to fission in several Ra isotopes with the neutron number $144 \leq N \leq 176$. Inner and outer barrier heights as well as first and second isomer excitation energies are given. The existence of a well developed third minimum along the fission paths of Ra nuclei, is analyzed in terms of the energetics of the "fragments" defining such elongated configuration. The masses and charges of the fission fragments are studied as functions of the neutron number in the parent Ra isotope. The comparison between fission and α -decay half-lives, reveals that the former becomes faster for increasing neutron numbers. Though there exists a strong variance of the results with respect to the parameters used in the computation of the spontaneous fission rate, a change in tendency is observed at $N=164$ with a steady increase that makes heavier neutron-rich Ra isotopes stable against fission, diminishing the importance of fission recycling in the r-process.

PACS numbers: 24.75.+i, 25.85.Ca, 21.60.Jz, 27.90.+b, 21.10.Pc

I. INTRODUCTION.

Fission is a very challenging kind of collective motion whose theoretical description can be addressed in terms of the evolution of a given nuclear system from its ground state to scission. To simplify this view such evolution is described in terms of several intrinsic shapes, labeled by the corresponding deformation parameters [1–4]. The precise description of both the fission energy landscape and the associated shell effects remains as a major challenge in nuclear structure physics, with a potential impact on several basic research and technological areas.

A detailed knowledge of the fission mechanism is required, for example, to better understand the very limits of the nuclear stability. As one goes up in atomic number Z , the stability of the nucleus against fission tends to decrease, due to the increasing Coulomb repulsion, and the quantum mechanical shell effects are the only mechanism to increase the chances of survival of a given element [5–8].

Fission properties of neutron-rich heavy nuclei are also relevant in the nucleosynthesis and abundances of elements with mass number greater than 120 due to competing fission recycling in the r-process in scenarios involving long neutron exposures [9–11]. Although induced fission is the process to understand, a preliminary description of the potential energy surfaces and spontaneous fission lifetimes of the involved nuclei can shed some light into the problem. Also, systematic studies of the fission paths and related properties, based on complementary theoretical approaches, are very useful to deepen our knowledge of the different decay channels (fission, α -decay, ...) and their competition in heavy and super-heavy nuclei (see, for example, [12–16] and references therein). On the other hand, observables like the half-lives, fragment mass and kinetic energy distributions are sensitive to the

topography of the fission landscape. In turn, an improvement in the computation of those quantities would be very useful to determine the upper end of the nucleosynthesis flow [17].

In addition to the physics already mentioned, nuclear fission remains a topic of high interest for reactor physics, the degradation of radioactive waste, prompt neutron-capture data from weapon tests as well as in the context of the progress made in recent years in the production of super-heavy elements (see, for example, [1, 3, 18–20] and references therein).

With all this in mind, we have carried out fission calculations for the radium isotopes from the stability line to very neutron rich isotopes in order to study the evolution of the potential energy surfaces and spontaneous fission lifetimes. This work can be considered as a complement to our previous fission studies in neutron-rich U and Pu isotopes [14, 15]. As a side product of the calculations, several examples of second fission isomers have been found.

From the theoretical point of view several models are used to describe nuclear fission. Among them, both macroscopic-microscopic [20–26] and mean-field [8, 16, 27–36] ones are common choices. The approximation employed in this work belongs to the second class, i.e., the Hartree-Fock-Bogoliubov (HFB) [37] framework based on the highly predictive parametrizations D1S [38], D1N [39] and D1M [40] of the Gogny [41] energy density functional (EDF). In this kind of studies, the potential energy surfaces (PES) of the different paths to fission, the associated collective masses and zero-point quantum corrections provided by the mean-field calculations, have been used to compute the spontaneous fission half-lives t_{SF} as well as a first approach to the masses and charges of the fission fragments based on energetics. Special attention has been paid to the uncertainties in the computation

of the spontaneous fission half-lives and the impact of pairing correlations on observables. For recent complementary work, based on the BCPM-EDF [42], the reader is referred to [16, 43].

In this paper, we focus on the fission properties of even-even Ra isotopes with neutron numbers $144 \leq N \leq 176$ in order to examine to which extent the main features found for the neutron-rich U and Pu nuclei are still preserved down to $Z=88$. With the aim to evaluate the robustness of our predictions, HFB calculations based on the D1S, D1N and D1M parametrizations of the Gogny-EDF have been performed. It should be kept in mind, that the D1N [39] and D1M [40] EDFs provide a better description of the nuclear masses, an aspect of relevance to the evaluation of the competing α decay channel. In addition, those EDFs were fitted using information on neutron matter and therefore they are expected to perform well when extrapolating to neutron-rich systems like the ones considered in the present study. On the other hand, the thoroughly tested Gogny-D1S [38] EDF, already successfully applied to fission studies in heavy and super-heavy nuclei [8, 27, 29], has been taken as a reference in this work. This will allow us to test the performance of the D1N and D1M Gogny-EDFs scarcely used in fission calculations up to now. We implicitly assume that the fission properties are determined by general features of the considered Gogny-EDFs and therefore, no fine tuning has been carried out.

The paper is organized as follows. In Sec. II, we briefly outline our theoretical framework. The results obtained for the fission paths, barrier heights, fission isomers, fragments' mass and charge in $^{232-264}\text{Ra}$ as well as the isotopic dependence of the spontaneous fission half-lives and the competition with the α -decay mode are discussed in Sec. III. Special attention has been paid, in the same section, to second fission isomers (i.e., third minima) along the fission paths of the considered nuclei. Such minima have been found for several U and Pu nuclei in our recent HFB studies [14–16] and have attracted considerable attention [25–27, 32, 44–53]. Finally, Sec. IV is devoted to the conclusions and work perspectives.

II. THEORETICAL FRAMEWORK

In this section, we briefly outline the theoretical framework used in the present study. A detailed account of our methodology can be found in [14–16].

The main ingredient is the HFB approximation [37], that is used with constraints on the axially symmetric quadrupole \hat{Q}_{20} and octupole \hat{Q}_{30} operators [14–16, 43, 54, 55] to obtain one-fragment (1F) solutions. We are aware of the role played by triaxiality for configurations around the top of the inner barrier [14, 27, 34]. However, we have kept axial symmetry, as a selfconsistent symmetry, along the whole fission path in order to reduce the already substantial computational effort. The γ degree of freedom has also been neglected in the com-

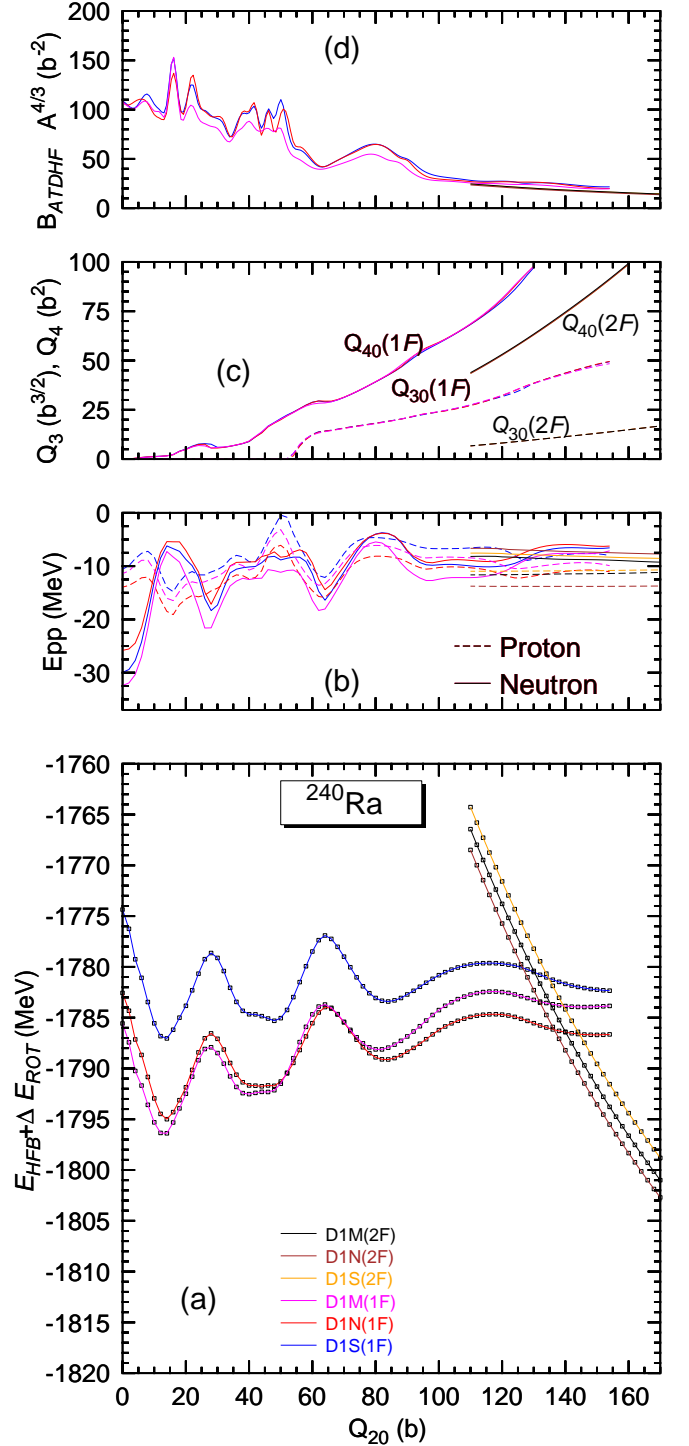


FIG. 1: (Color online) The HFB plus the zero point rotational energies obtained with the D1S, D1N and D1M Gogny-EDFs are plotted in panel (a) as functions of the quadrupole moment Q_{20} for the nucleus ^{240}Ra . For each EDF, both the one (1F) and two-fragment (2F) solutions are included in the plot. The pairing interaction energies are depicted in panel (b) for protons (dashed lines) and neutrons (full lines). The octupole and hexadecapole moments corresponding to the 1F and 2F solutions are given in panel (c). The collective masses obtained within the ATDHF approximation are plotted in panel (d). For more details, see the main text.

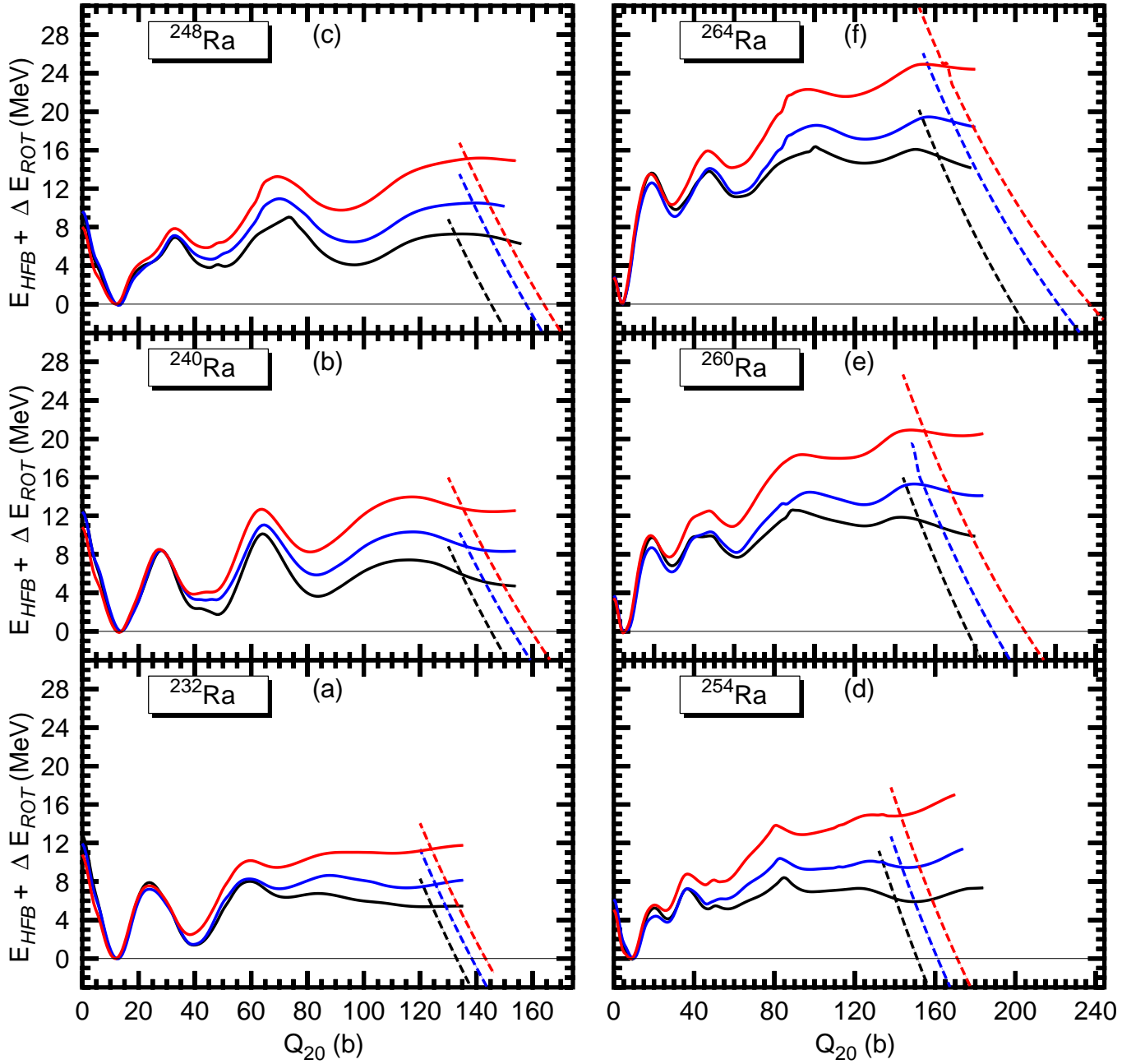


FIG. 2: (Color online) The one-fragment (full lines) and two-fragment (dashed lines) HFB plus the zero point rotational energies obtained with the D1S (black), D1N (blue) and D1M (red) parametrizations of the Gogny-EDF are plotted for the nuclei ^{232}Ra [panel (a)], ^{240}Ra [panel (b)], ^{248}Ra [panel (c)], ^{254}Ra [panel (d)], ^{260}Ra [panel (e)] and ^{264}Ra [panel (f)] as functions of the quadrupole moment Q_{20} . All the relative energies are referred to the absolute minima of the corresponding one-fragment curves. For more details, see the main text.

putation of our t_{SF} values [see, Eqs.(1) and (2) below] as it has been shown in previous studies [6, 56] that its impact is very limited.

For large values of the quadrupole moment Q_{20} , two-fragment (2F) solutions have been reached by constraining on the necking operator $\hat{Q}_{\text{Neck}}(z_0, C_0)$. In computing spontaneous fission lifetimes (see below) the ridge connecting the 1F and 2F curves in the multidimensional

space of deformations ($Q_{20}, Q_{30}, Q_{\text{Neck}}, \dots$) has been neglected and therefore the 2F curves are considered as really intersecting the 1F ones [14–16].

Aside from the constraints already mentioned, as well as the typical HFB ones on both the proton and neutron numbers [37], a constraint on the operator \hat{Q}_{10} is used to prevent spurious effects associated to the center of mass motion [54, 55]. Note, that the average values of higher

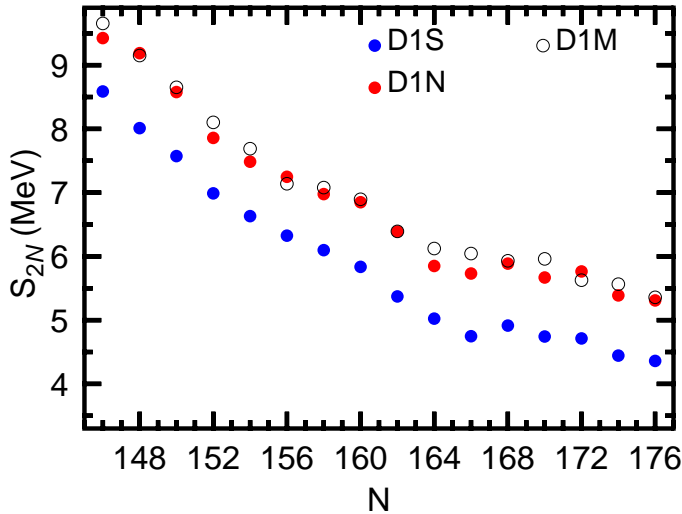


FIG. 3: (Color online) Two neutron separation energies S_{2N} as functions of the neutron number.

multipolarity deformations (i.e., \hat{Q}_{40} , \hat{Q}_{60} , ...) are automatically adjusted during the selfconsistent minimization of the HFB energies. Furthermore, as a result of projecting multidimensional paths into one-dimensional plots (see, Figs. 1 and 2) kinks and multiple branches may appear in this type of calculations [14–16, 57].

The HFB quasiparticle operators are expanded in a deformed axially symmetric harmonic oscillator (HO) basis with quantum numbers restricted by the condition $2n_{\perp} + |m| + \frac{1}{q}n_z \leq M_{z,\text{MAX}}$ where $M_{z,\text{MAX}}=17$ and $q = 1.5$. This amounts to consider states with J_z quantum numbers up to $35/2$ and up to 26 quanta in the z -direction. For a neutron-rich nucleus like ^{280}Pu this basis provides an error (with respect to a larger basis with $M_{z,\text{MAX}}=18$) smaller than 0.8 MeV all over the fission path [15]. In addition, for each of the considered $(Q_{20}, Q_{30}, Q_{\text{Neck}}, \dots)$ -configurations, the HO lengths b_{\perp} and b_z have been optimized so as to minimize the total HFB energy. This guarantees a much better convergence for relative energies (see, Fig.2).

For the solution of the constrained mean-field equations we have employed an approximate second order gradient method based on the parametrization of a given HFB vacuum with the help of the Thouless theorem [54, 55, 58]. The two-body kinetic energy correction has been fully taken into account in the Ritz-variational [37] procedure while for the Coulomb exchange term we have considered the Slater approximation. The spin-orbit contribution to the pairing field has been neglected.

We have computed the spontaneous fission half-life using the Wentzel-Kramer-Brillouin (WKB) formalism [59, 60]

$$t_{\text{SF}} = 2.86 \times 10^{-21} \times (1 + e^{2S}) \quad (1)$$

where the action S along the (minimal energy one-

dimensional projected) fission path reads

$$S = \int_a^b dQ_{20} \sqrt{2B(Q_{20}) (V(Q_{20}) - (E_{\text{GS}} + E_0))}. \quad (2)$$

In the above expression, $B(Q_{20})$ and $V(Q_{20})$ represent the collective mass and potential for the collective variable Q_{20} . The potential energy is given by the HFB energy of the corresponding constrained state corrected by the quantum zero point vibrational $\Delta E_{\text{vib}}(Q_{20})$ and rotational $\Delta E_{\text{ROT}}(Q_{20})$ energies. Both the inertia $B(Q_{20})$ and $\Delta E_{\text{vib}}(Q_{20})$ have been computed using the cranking approximation to the Adiabatic Time Dependent HFB (ATDHFB) approach [61–64] and the Gaussian Overlap Approximation (GOA) to the Generator Coordinate Method (GCM) [14–16, 37] while $\Delta E_{\text{ROT}}(Q_{20})$ has been computed in terms of the Yoccoz moment of inertia [65, 66]. The integration limits a and b in Eq. (2) are the classical turning points [67] corresponding to the energy $E_{\text{GS}} + E_0$. For the free parameter E_0 , we have considered the four values $E_0=0.5, 1.0, 1.5$ and 2.0 MeV in order to study its impact on lifetimes. It should be kept in mind that different E_0 values lead to different integration limits and, therefore, modify the value of the integral in Eq. (2). This is particularly relevant, in the case of neutron-rich Ra isotopes which display high and wide fission barriers.

Finally, in order to study the competition between the spontaneous fission and α -decay modes, we have computed the corresponding t_{α} values using the Viola-Seaborg formula

$$\log_{10} t_{\alpha} = \frac{AZ + B}{\sqrt{Q_{\alpha}}} + CZ + D \quad (3)$$

with the parameters $A=1.64062$, $B=-8.54399$, $C=-0.19430$ and $D=-33.9054$ as given in [13]. The Q_{α} value is obtained from the calculated binding energies for Ra and Rn nuclei. Obviously, other types of decay (for example, β -decay) may play a role in the case of heavy neutron-rich nuclei. However, their study lies outside the scope of this work.

III. DISCUSSION OF THE RESULTS

An illustrative outcome of our calculations is presented in Fig.1 for the nucleus ^{240}Ra . A similar analysis, as described below, has been carried out for each of the studied Ra isotopes. In panel (a), we have plotted the HFB energies plus the rotational corrections $E_{\text{HFB}} + \Delta E_{\text{ROT}}$ as functions of the quadrupole moment. The zero point vibrational energies are not included in the plot, as they are rather constant as functions of Q_{20} . However, they are always included in the computation of the spontaneous fission half-lives.

As can be seen, the Gogny-D1S EDF provides a pronounced under-binding as compared to the D1N and D1M ones. This reflects a well known deficiency of the former in heavier nuclei [14, 15, 68] as a result of which

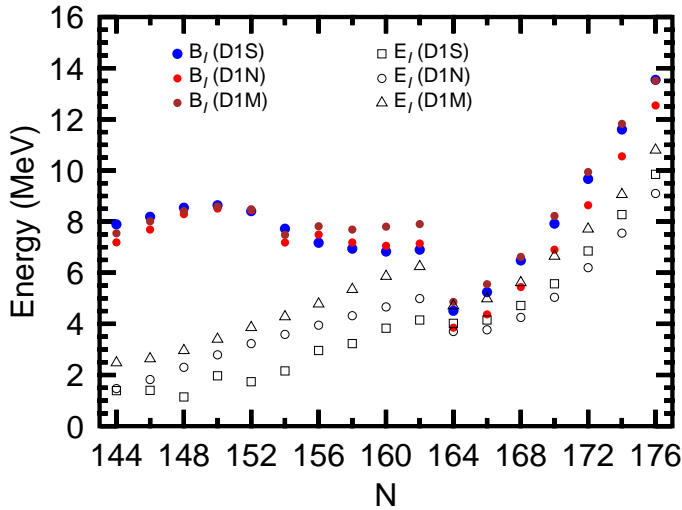


FIG. 4: (Color online) Excitation energies E_I of the first fission isomers and inner barrier heights B_I as function of the neutron number in $^{232-264}\text{Ra}$.

both the D1N and D1M parametrizations have been specially tailored in an effort to build an accurate mass table based on the Gogny-EDF [39, 40]. A similar behavior has been found in our symmetry-projected configuration mixing study of the quadrupole collectivity across the $N=126$ neutron shell closure [69] as well as in [70]. Nevertheless, it is satisfying to observe that the 1F curves provided by all the functionals are rather similar with the ground state at $Q_{20}=14$ b.

The first fission isomer appears at $Q_{20}=48, 44$ and 40 b with the D1S, D1N and D1M parametrizations. Their excitation energies are 1.74, 3.23 and 3.86 MeV, respectively. They are separated from the ground state by inner barriers with heights (without triaxiality) of 8.41, 8.44 and 8.48 MeV, respectively. Second fission isomers ($Q_{20} \approx 82$ b) are also apparent from panel (a). They lie 3.63, 5.87 and 8.26 MeV above the ground state while the heights of the second barriers ($Q_{20} \approx 64$ b) are 10.13, 11.03 and 12.67 MeV with the D1S, D1N and D1M parametrizations. Reflection-asymmetric second fission isomers, have already been found in previous studies [14–16, 25–27, 32, 47–53]. As will be shown later on (see, Fig. 2) they also emerge along the fission paths of several Ra isotopes.

The proton (dashed lines) and neutron (full lines) pairing correlation energies $E_{pp}=1/2 \text{Tr}(\Delta\kappa^*)$ are shown in panel (b). Minima are observed for the neutron pairing energies at the spherical configuration, the top of the inner and second barriers as well as for $Q_{20} \approx 100$ b. In panel (c), we have plotted the octupole Q_{30} and hexadecupole Q_{40} moments corresponding to the 1F [i.e., $Q_{30}(1F)$ and $Q_{40}(1F)$] and 2F [i.e., $Q_{30}(2F)$ and $Q_{40}(2F)$] paths which are clearly separated in the multidimensional (collective) deformation space and rather similar for all the parametrizations.

The ATDHFB collective masses are displayed in panel

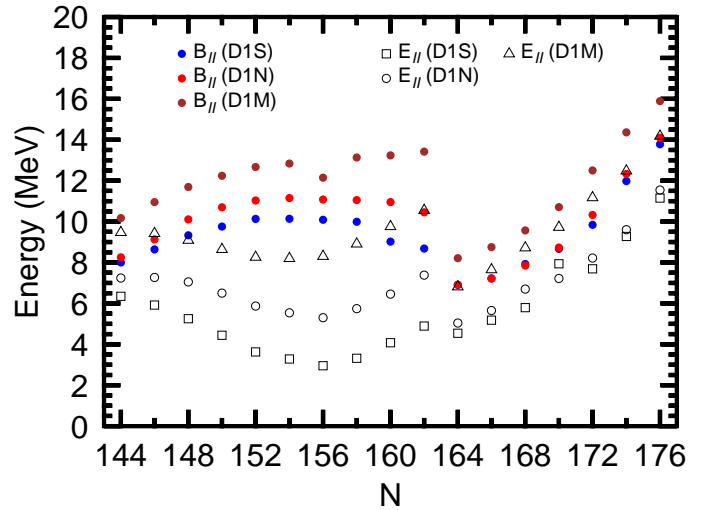


FIG. 5: (Color online) Excitation energies E_{II} of the second fission isomers and second barrier heights B_{II} as function of the neutron number in $^{232-264}\text{Ra}$.

(d). Their behavior is well correlated with the one for the pairing energies shown in panel (b) and the inverse dependence of the collective mass with the square of the pairing gap [67, 71]. The GCM collective masses (not shown in the figure) display a similar pattern though they are smaller than the ATDHFB ones. For ^{240}Ra and $E_0=1.0$ MeV, for example, this leads to pronounced differences of 10, 12 and 13 orders of magnitude in the t_{SF} values predicted in the two schemes with the D1S, D1N and D1M parameter sets, respectively. These large uncertainties, are one of the main reasons driving our choice of both schemes in the computation of the spontaneous fission half-lives. In all the computations of the t_{SF} values, the wiggles in the collective masses have been softened by means of a three point filter [14].

Let us also mention that, for large quadrupole moments, the 2F solutions in ^{240}Ra correspond to a spherical ^{130}Cd and an oblate ($\beta_2=-0.21$) and slightly octupole deformed ($\beta_3=0.03$) ^{110}Zr fragment. With the D1S, D1N and D1M Gogny-EDFs, the oblate ^{110}Zr fragment minimizes Coulomb repulsion energies of 166.31, 166.34 and 166.55 MeV, respectively. Oblate fragments have also been found by fissioning other Ra (see, below), U and Pu [14–16] nuclei. Here, we would like to stress that fragment masses are the result of the minimization of the HFB energy at a given distance between the fragments and therefore should only be taken as rough approximations to the peaks of the broad fragments' mass distribution [72]. The heavier fragment, ^{130}Cd , is a consequence of its neutron number $N=82$ being a magic number [15, 73–75]. A more realistic description of fragments' mass distribution [76, 77] has to take into account the dynamics of the system around the loosely defined scission configuration [14, 15, 78].

In Fig. 2 we have plotted the energies $E_{HFB} + \Delta E_{ROT}$, as functions of the quadrupole moment Q_{20} , for ^{232}Ra ,

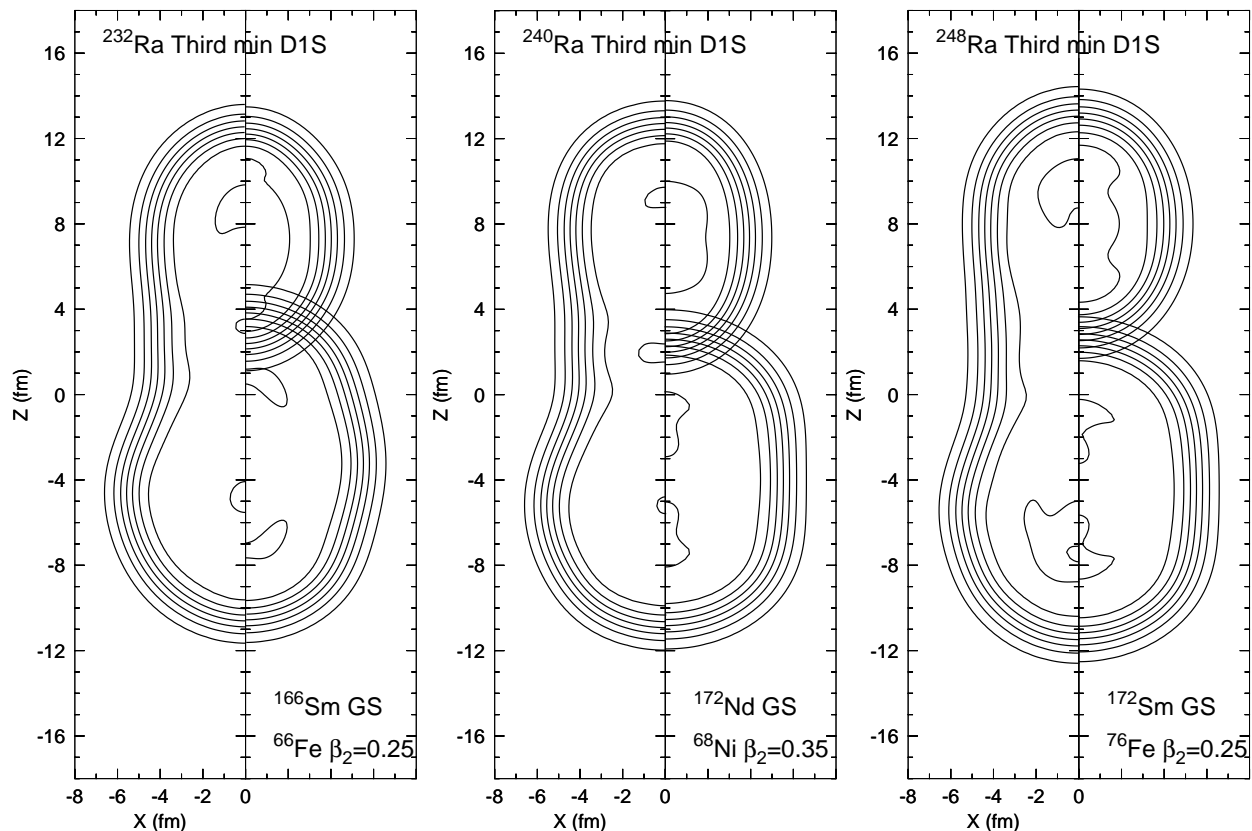


FIG. 6: The spatial density (left hand side of each panel) corresponding to the second isomer in the nuclei ^{232}Ra , ^{240}Ra and ^{248}Ra is compared to the densities (right hand side of each panel) of two nuclei summing up the same number of protons and neutrons as the parent nucleus. The density is in units of fm^{-3} . Results are shown for the Gogny-D1S EDF. For more details, see the main text.

^{240}Ra , ^{248}Ra , ^{254}Ra , ^{260}Ra and ^{264}Ra as a representative sample of the considered isotopes. Both the 1F (full lines) and 2F (dashed lines) paths are shown in the plots. For each isotope the relative energies are always referred to the absolute minima of the 1F curves in order to accommodate all the paths, obtained with the D1S, D1N and D1M Gogny-EDFs, in a single plot. Results for ^{240}Ra are also included in the figure for the sake of completeness.

The ground state deformation decreases with increasing neutron number N reaching its minimal value $Q_{20}=2\text{b}$ for ^{264}Ra . Using the corresponding ground state energies, we have computed the two-neutron separation energies S_{2N} shown in Fig. 3. Regardless of the considered functional, the S_{2N} values exhibit a clear decreasing trend with increasing neutron number. In the case of ^{234}Ra we have obtained $S_{2N}=8.59, 9.42$ and 9.66 MeV with the D1S, D1N and D1M parametrizations while for ^{264}Ra the corresponding two-neutron separation energies are $S_{2N}=4.36, 5.48$ and 5.36 MeV, respectively. The smaller S_{2N} values obtained with the D1S as compared with the D1N and D1M parametrizations (typically around 1 MeV) are due to the well known underbinding of the D1S parametrization.

The excitation energies E_I of the first fission isomers and the inner barrier heights B_I (without triaxiality) are

summarized in Fig. 4. With all the functionals, the E_I values increase almost linearly as functions of the neutron number exception made of ^{252}Ra (4.02, 3.70 and 4.71 MeV with the D1S, D1N and D1M Gogny-EDFs) for which a change in tendency is observed. The barrier heights B_I reach their minimal values (4.51, 3.85 and 4.86 MeV with the D1S, D1N and D1M Gogny-EDFs) for the $N=164$ nucleus ^{252}Ra and increase for heavier isotopes. Such an increase agrees well with the HFB predictions for neutron-rich U and Pu nuclei [14–16] and previous Extended Thomas-Fermi (ETF) results [79]. An increase is also visible in the recently reported macroscopic-microscopic B_I values for even-even Ra isotopes with $166 \leq N \leq 182$ [20]. Larger B_I values, together with the widening of the 1F curves, leads to larger spontaneous fission half-lives as one moves towards more neutron-rich systems (see, Fig. 9).

We are aware of the reduction, by a few MeV, of the inner barrier heights B_I once triaxiality is taken into account (see, for example [34]). In fact, such a reduction has already been found in our previous Gogny-D1M HFB calculations for a set of U, Pu, Cm and Cf nuclei (see Table I and Fig. 4 of [14]). Though we have mainly kept axial symmetry along the fission paths of the considered Ra isotopes, we have also corroborated in some selected

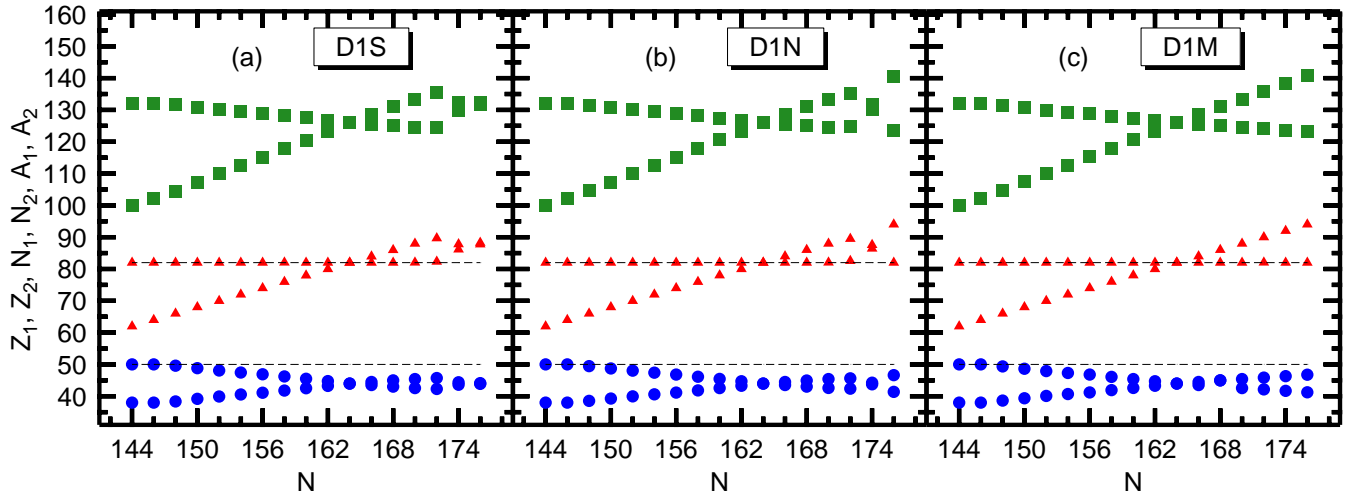


FIG. 7: (Color online) The proton (Z_1, Z_2), neutron (N_1, N_2) and mass (A_1, A_2) numbers of the two fragments obtained in our HFB calculations for the isotopes $^{232-264}\text{Ra}$ are shown as functions of the neutron number in the parent nucleus. Results have been obtained with the Gogny-D1S [panel (a)], Gogny-D1N [panel (b)] and Gogny-D1M [panel (c)] EDFs. The magic proton $Z=50$ and neutron $N=82$ numbers are highlighted with dashed horizontal lines to guide the eye.

cases (i.e., ^{232}Ra , ^{236}Ra and ^{244}Ra) the reduction of the corresponding B_I values once the γ degree of freedom is included. However, such a reduction comes together with an increase of the collective inertia [56, 80] that tends to compensate in the final value of the action. As a result, the impact of the γ degree of freedom is very limited and has not been considered in our calculations of the spontaneous fission half-lives.

Coming back to Fig. 2, one also observes another common feature provided by all the the Gogny-EDFs, i.e., second fission isomers in the 1F curves of the studied Ra nuclei. For the isotopes $^{232-252}\text{Ra}$ their quadrupole deformations are within the range $68 \text{ b} \leq Q_{20} \leq 102 \text{ b}$. They are also apparent in the 1F curves of the heavier isotopes though in that case additional shallow minima have been found.

The second barrier heights B_{II} and the excitation energies E_{II} of the second fission isomers are summarized in Fig. 5. Though all the considered functionals provide a similar trend, the largest barrier heights B_{II} are obtained with the D1M parametrization. A sudden drop in the B_{II} values occurs for the $N=164$ isotope ^{252}Ra (6.90, 6.92 and 8.21 MeV with the D1S, D1N and D1M Gogny-EDF) followed by an almost linear increase in heavier isotopes. Note, that for neutron numbers $N \geq 164$, the predicted D1S and D1N B_{II} values are rather close (see, Fig. 2). The largest E_{II} energies are also the ones obtained with the Gogny-D1M EDF. Here, one observes two minima (one at $N=156$ and the other at $N=164$ regardless of the EDF employed) and a steady increase in heavier isotopes for which the corresponding D1S and D1N E_{II} values are, once more, rather close (see, Fig. 2).

The previous results for E_I , E_{II} , B_I and B_{II} agree well with the ones obtained for U and Pu nuclei [14, 15]. In particular, one sees that, regardless of the employed

functional, third minima along the fission paths represent a robust feature within our Gogny-HFB framework. They are also visible in the 1F curves of the isotopes $^{232-254}\text{Th}$ for which preliminary calculations have been carried out. The same conclusions can be extracted from recent BCPM [16], Skyrme [32] and relativistic mean-field [53] studies. Therefore, the shell effects leading to second fission isomers (i.e., third minima) in this region of the nuclear chart are systematically present in all the mean-field approximations already mentioned. However, further studies are required in order to clarify the relation between the mean-field predictions and the available experimental data.

In order to further understand the origin of the extra stability leading to second fission isomers, we have performed a similar analysis to the one of [32] where the spatial density for that second isomer is compared to the densities of two nuclei summing up the same number of protons and neutrons as the parent nucleus. In order to choose the N and Z values used, we plot the number of particles $N(z) = 2\pi \int_{-\infty}^z dz' \int r_{\perp} dr_{\perp} \rho(r_{\perp}, z')$ up to a distance z . This quantity has several regions where it behaves quadratically with z and a central region (corresponding to the neck) where it behaves almost linearly. By locating the mid point of that region of linear growing, we determine the Z and N values mentioned above. A subsequent HFB calculation for the ground state or an excited configuration (see below) allows to obtain the corresponding densities that are then shifted as to match the tips of the density of the parent nucleus. In Fig. 6, we have plotted the density (left hand side of each panel) corresponding to the second fission isomer in ^{232}Ra , ^{240}Ra and ^{248}Ra and the densities (right hand side of each panel) of the two nuclei described above. In each panel the corresponding splitting is given in the lower

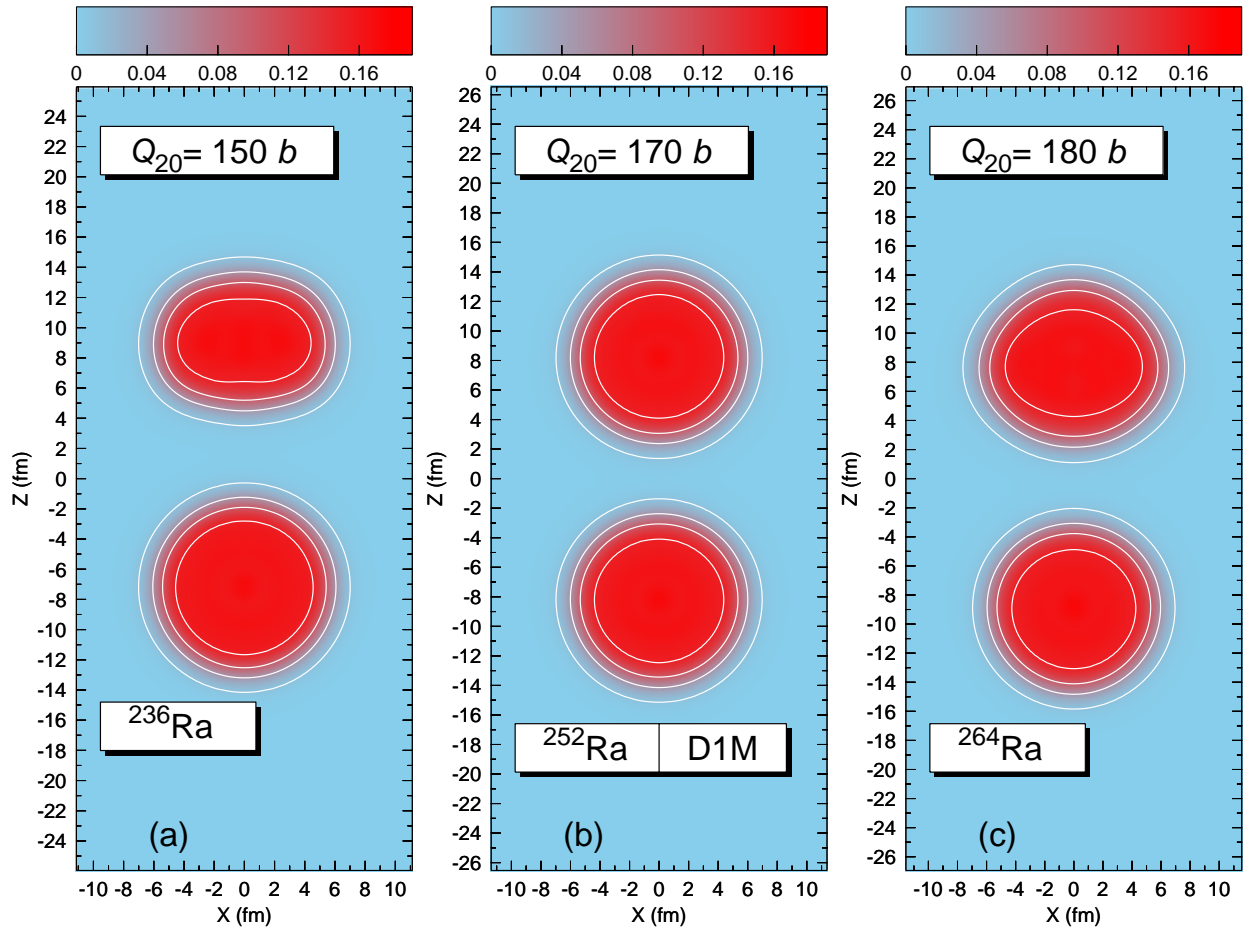


FIG. 8: (Color online) Density contour plots for the nuclei ^{236}Ra [panel (a)], ^{252}Ra [panel (b)] and ^{264}Ra [panel (c)]. The density profiles correspond to 2F solutions at the quadrupole deformations $Q_{20}=150, 170$ and 180 b, respectively. Results are shown for the parametrization D1M of the Gogny-EDF. The density is in units of fm^{-3} and contour lines are drawn at 0.01, 0.05, 0.10 and 0.15 fm^{-3} .

part. The densities computed with the D1S, D1N and D1M Gogny-EDFs are quite similar and therefore, we will focus on the results obtained with the D1S parameter set. The densities of the three nuclei show some differences as a consequence of the different number of protons and neutrons as well as the different quadrupole moment but qualitatively they look rather similar pointing to a weak dependence with neutron number. With respect to the "fragments", the heavier one is always a rare earth nucleus with a prolate deformation in its ground state. The light "fragment" is characterized by its proton number close or equal to the magic $Z = 28$ one, that leads to a spherical ground state. In spite of being spherical, the three light "fragments" have a quadrupole potential energy surface showing a shoulder at $\beta_2 \approx 0.25 - 0.35$ with an excitation energy of just a couple MeV. The density of that "excited configuration" matches quite well the density of the second isomer and therefore the existence of the third minimum could be linked to shell effects in the light system associated to the above mentioned shoulder. This finding has to be confirmed by a similar analysis

in other Th, U and Pu nuclei showing a second fission isomer.

Let us turn our attention, to the proton (Z_1, Z_2), neutron (N_1, N_2) and mass (A_1, A_2) numbers of the fragments obtained at the HFB level in $^{232-264}\text{Ra}$ which are plotted in Fig. 7. As can be seen the overall trend is quite reminiscent of the one in U and Pu nuclei [14, 15]. The key role played by the magic neutron and proton numbers in the fragments' masses and charges is also apparent from the figure. For example, exception made of the isotopes $^{262, 264}\text{Ra}$ with the parametrizations D1S and D1N, the neutron number in one of the fragments is always rather close or equal to 82. Moreover, for $^{232-244}\text{Ra}$, the proton number in one of the fragments is close to 50 which compares well with available experimental data for this region of the nuclear chart [81]. We stress, however, that such a comparison with the experiment should be taken with care because, as already discussed above for the case of ^{240}Ra , in our calculations the masses and charges of the fragments are obtained from HFB 2F solutions minimizing the energy at the largest quadrupole

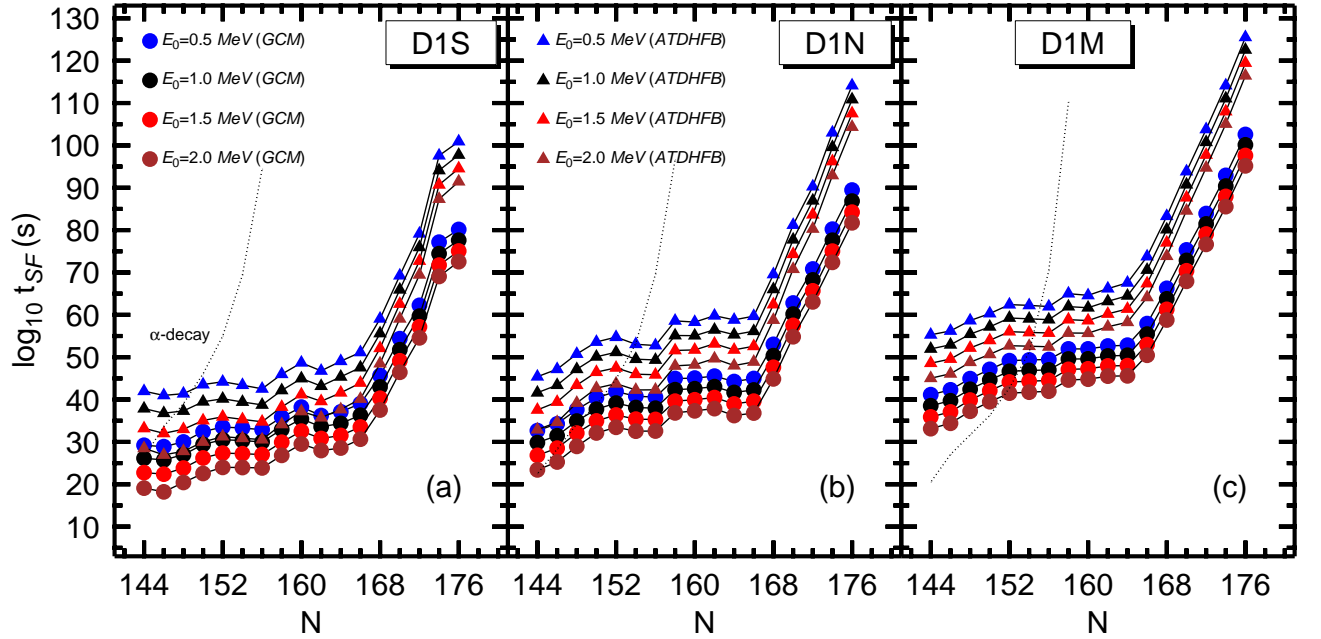


FIG. 9: (Color online) The spontaneous fission half-lives t_{SF} , predicted within the GCM and ATDHFB schemes, for the isotopes $^{232-264}\text{Ra}$ are depicted as functions of the neutron number. Results have been obtained with the Gogny-D1S [panel (a)], Gogny-D1N [panel (b)] and Gogny-D1M [panel (c)] EDFs. For each parametrization, calculations have been carried out with $E_0=0.5, 1.0, 1.5$ and 2.0 MeV, respectively. The α -decay half-lives are also plotted with short dashed lines.

deformations.

In Fig. 8 we have plotted the 2F density contours for the nuclei ^{236}Ra , ^{252}Ra and ^{264}Ra at $Q_{20}=150, 170$ and 180 b, respectively. Results are shown for the Gogny-D1M EDF but similar ones are obtained with the D1S and D1N parametrizations. The lighter and heavier fragments in ^{236}Ra and ^{264}Ra turn out to be oblate ($\beta_2=-0.23$ and -0.14 , respectively). In fact, our calculations predict, for example, oblate ($-0.26 \leq \beta_2 \leq -0.17$) and slightly octupole ($\beta_3 \approx 0.03$) deformed lighter fragments for the isotopes $^{232-244}\text{Ra}$. Such oblate fragments have also been found in previous HFB calculations based on both the Gogny and BCPM EDFs [14–16]. A better understanding of the shell effects leading to them is required as only prolate deformations are usually assumed for the fission fragments [21, 22]. On the other hand, a symmetric splitting into two ^{126}Ru nuclei ($\beta_2=-0.02, \beta_3 \approx 0.01$) is predicted for ^{252}Ra . The same holds for the $N=164$ nuclei ^{256}U [14] and ^{258}Pu [15] (two ^{128}Pd and ^{129}Ag fragments, respectively). Moreover, our calculations for ^{254}Th suggest a splitting into two ^{127}Rh fragments.

Finally, in Fig. 9, we have depicted the spontaneous fission half-lives obtained for $^{232-264}\text{Ra}$ as functions of the neutron number. Both the GCM and ATDHFB schemes have been employed. For each isotope we have considered four values of E_0 (i.e., $E_0=0.5, 1.0, 1.5$ and 2.0 MeV) and, as can be seen from the figure, an increase of this parameter leads to a decrease in the t_{SF} values by several orders of magnitude. On the other hand, the ATDHFB half-lives are always larger than the GCM ones for a given E_0 . For example, for ^{234}Ra (^{252}Ra) the GCM values are

5.492×10^{25} (2.243×10^{34}), 2.951×10^{31} (4.578×10^{41}) and 5.247×10^{39} (2.755×10^{50}) s while ATDHFB ones are 5.884×10^{36} (2.293×10^{45}), 2.513×10^{43} (1.992×10^{55}) and 8.511×10^{52} (3.094×10^{64}) s with the D1S, D1N and D1M Gogny-EDFs and $E_0=1.0$ MeV. In fact, for the isotopes with $N \leq 166$, we have found differences of up to 11, 14 and 15 orders of magnitude between the two schemes. We observe a steady increase of the t_{SF} values in heavier isotopes, with the differences between the GCM and ATDHFB predictions reaching 20, 24 and 22 orders of magnitude in the case of ^{264}Ra with the D1S, D1N and D1M parameter sets ($E_0=1.0$ MeV). The conclusion is that t_{SF} values strongly depend upon the details of the calculation and the functional used with “error bars” of up to 20 orders of magnitude. However, a global trend is observed in *all* the cases, i.e., the slight increase of t_{SF} as a function of neutron number up to $N=166$ which is followed by a steeper increase that continues up to the largest neutron number considered, ruling out the possibility of fission recycling in the r-process. In order to examine the competition between the spontaneous fission and α -decay modes, in Fig. 9 we have also included the α -decay half-lives Eq.(3). Though the precise transition point depends of the selected Gogny-EDF, we conclude that with increasing neutron number fission turns out to be faster than α -decay.

As expected, pairing correlations have a strong impact on the spontaneous fission half-lives obtained for the considered Ra nuclei. We have tested that, similar to previous Gogny and/or BCPM results [14–16], an increase of the pairing field by only 5 or 10 % leads to a sig-

nificant decrease in the predicted t_{SF} values. However, even in such a case, the previous conclusion (i.e., fission dominates over α -decay for increasing N) remains valid regardless of the Gogny-EDF used in the calculations.

IV. CONCLUSIONS

In the present work, we have studied the fission properties of even-even Ra isotopes with neutron numbers $144 \leq N \leq 176$ within a mean field framework [37]. With the aim to test the robustness of our HFB predictions with respect to the particular version of the Gogny-EDF [41] employed, calculations have been carried out with the parameter sets D1S [38], D1N [39] and D1M [40]. The fission paths (i.e., the 1F and 2F solutions) have been determined, for each Ra isotope, with the help of constraints on the proton \hat{Z} and neutron \hat{N} number operators as well as on the axially symmetric quadrupole \hat{Q}_{20} , octupole \hat{Q}_{30} , \hat{Q}_{10} and necking $\hat{Q}_{Neck}(z_0, C_0)$ operators. For each of the considered $(Q_{20}, Q_{30}, Q_{Neck}, \dots)$ -configurations we have also performed an optimization of the lengths of the (deformed) axially symmetric HO single-particle basis in order to improve the convergence of the relative energies [14–16]. The mean field equations have been solved using an approximate second order gradient method that allows to handle several constraints efficiently [54, 55, 58]. Zero point vibrational and rotational corrections have always been added to both the 1F and 2F HFB energies.

Regardless of the considered Gogny-EDF, the 1F curves of the studied Ra nuclei exhibit a similar rich topography consisting of, for example, the ground state minimum, first and second fission isomers as well as first and second barriers. A change in tendency is observed for the excitation energies of the first E_I and second E_{II} isomers as well as for the heights of the first B_I and second B_{II} barriers at the neutron number $N=164$. For some selected Ra isotopes, we have also corroborated the expected reduction of the inner barrier heights B_I [14, 15, 34] once the γ degree of freedom is taken into account. Moreover, in order to better understand the structure of the third minima along the 1F curves, we have studied their density profiles. Ours agree well with previous results [32] and suggest that those third minima in Ra nuclei could be linked to shell effects associated with an excited (deformed) configuration in a light (spherical) system with $Z \approx 28$. A more detailed study, including other Th, U and Pu nuclei showing a second fission isomer, will be presented elsewhere.

We have obtained the masses and charges of the fission fragments, from (variational) 2F solutions at the largest quadrupole moments. A symmetric splitting into two ^{126}Ru nuclei is predicted for ^{252}Ra as well as oblate and slightly octupole deformed fission fragments for several other Ra isotopes. Though the predicted overall trend for the fragments' masses and charges agrees reasonably well with available data [81] for this region of the nuclear

chart, we stress that our procedure tends to overestimate [14, 15] the role of the proton $Z=50$ and neutron $N=82$ magic numbers [73–75]. Therefore, a more sophisticated [72] approach, taking into account the quantum dynamics around the scission configurations [78], is still required.

The spontaneous fission half-lives t_{SF} have been computed within the standard WKB approximation [59, 60]. Both the ATDHFB [61–64] and the GCM [14–16, 37] schemes have been employed to obtain the collective masses and the zero point vibrational corrections while for the rotational energies we have resorted to an approximate variation-after-projection (VAP) [37] in terms of the Yoccoz moment of inertia [65, 66]. In spite of the large uncertainties in the predicted t_{SF} values, mainly related to the details of the calculations (including the strength of pairing correlations and the Gogny-EDF used) a robust global trend is observed, i.e., the slight increase of the t_{SF} values up to $N=166$ followed by a steady increase up to ^{264}Ra that correlates well with the one of the barrier heights and the widening of the 1F curves in heavier Ra isotopes. As a result, heavier neutron-rich Ra nuclei become stable against spontaneous fission, diminishing the importance of fission recycling in the r-process [9–11]. Furthermore, our calculations indicate that with increasing neutron number fission turns out to be faster than α -decay.

From the results discussed in this paper we conclude that the fission properties found for neutron-rich U and Pu [14–16] are preserved down to neutron-rich Ra nuclei. This motivates further explorations in this region of the nuclear chart using the Gogny-HFB framework. Within this context, a long list of tasks should be undertaken. Among them, the following two appear as our next plausible steps. First, a minimal action, instead of minimal energy, description of fission including pairing fluctuations [43] in addition to multipole moments [82] should receive more attention. However, a more realistic treatment of the vibrational mass parameters is still required within the framework presented in [43]. Here, we also refer the reader to the recent study [83] where coherent and time-feasible calculations of the vibrational masses have been envisioned using the Gogny-HFB plus the quasiparticle random-phase approximation (RPA). Second, the study of the fission properties in odd-A nuclei will provide valuable information on the predictive power of our Gogny-HFB approach to account for the larger t_{SF} values in those nuclear systems compared with the corresponding even-A neighbors (i.e., the hindrance factors) [2]. Here, the Gogny-HFB equal filling approximation (EFA) [84–86], represents a reasonable and computationally feasible starting point. Work along these lines is in progress.

Acknowledgments

The work of L. M. Robledo has been supported in part by MINECO grants Nos. FPA2012-34694, FIS2012-

-
- [1] H.J. Specht, *Rev. Mod. Phys.* **46**, 773 (1974).
- [2] S. Björnholm and J.E. Lynn, *Rev. Mod. Phys.* **52**, 725 (1980).
- [3] H.J. Krappe and K. Pomorski, *Theory of Nuclear Fission*, Lectures Notes in Physics, **838** (Springer, Berlin, 2012).
- [4] A. Baran, M. Kowal, P. -G. Reinhard, L. M. Robledo, A. Staszczak and M. Warda, arXiv:1503.01608 [nucl-th] (2015).
- [5] S. Ćwiok, P. -H. Heenen and W. Nazarewicz, *Nature* **433**, 705 (2005).
- [6] M. Bender, K. Rutz, P. -G. Reinhard, J. Maruhn and W. Greiner, *Phys. Rev. C* **60**, 034304 (1999).
- [7] P. Möller, J. R. Nix, W. D. Myers and W. J. Swiatecki, *At. Data Nucl. Data Tables* **59**, 185 (1995).
- [8] M. Warda and J.L. Egido, *Phys. Rev. C* **86**, 014322 (2012).
- [9] I.V. Panov *et al* *Nucl. Phys.* **A747**, 633 (2005).
- [10] G. Martínez-Pinedo *et al* *Prog. in Part. and Nucl. Phys.* **59**, 199 (2007).
- [11] I.V. Panov, I. Yu. Korneev and F.-K. Thielemann *Astron. Lett.* **34**, 189 (2008).
- [12] V.E. Viola Jr. and G.T. Seaborg, *J. Inorg. Nucl. Chem.* **28**, 741 (1966).
- [13] T. Dong and Z. Ren, *Eur. Phys. J. A* **26**, 69 (2005).
- [14] R. Rodríguez-Guzmán and L. M. Robledo, *Phys. Rev. C* **89**, 054310 (2014).
- [15] R. Rodríguez-Guzmán and L. M. Robledo, *Eur. Phys. J. A* **50**, 142 (2014).
- [16] S. A. Giuliani and L.M. Robledo, *Phys. Rev. C* **88**, 054325 (2013).
- [17] M. Arnould, S. Goriely and K. Takahashi, *Phys. Rep.* **450**, 97 (2007).
- [18] C. Wagemans, *The Nuclear Fission Process* (CRC Press, Boca Raton, 1991).
- [19] R. Julin, *Nucl. Phys. A* **834**, 15c (2010).
- [20] P. Möller, A. J. Sierk, T. Ichikawa, A. Iwamoto and M. Mumpower, *Phys. Rev. C* **91**, 024310 (2015).
- [21] P. Möller and A. Iwamoto, *Phys. Rev. C* **61**, 047602 (2000).
- [22] P. Möller, D.G. Madlan, A.J. Sierk and A. Iwamoto, *Nature* **409**, 785 (2001).
- [23] M. Kowal, P. Jachimowicz and A. Sobczewski, *Phys. Rev. C* **82**, 014303 (2010).
- [24] M. Kowal and A. Sobczewski, *Int. J. Mod. Phys. E* **18**, 914 (2009).
- [25] M. Kowal and J. Skalski, *Phys. Rev. C* **85**, 061302(R) (2012).
- [26] P. Jachimowicz, M. Kowal and J. Skalski, *Phys. Rev. C* **87**, 044308 (2013).
- [27] J.-P. Delaroche, M. Girod, H. Goutte and J. Libert, *Nucl. Phys. A* **771**, 103 (2006).
- [28] N. Dubray, H. Goutte and J.-P. Delaroche, *Phys. Rev. C* **77**, 014310 (2008).
- [29] M. Warda, J. L. Egido, L.M. Robledo and K. Pomorski, *Phys. Rev. C* **66**, 014310 (2002).
- [30] N. Nikolov, N. Schunck, W. Nazarewicz, M. Bender and J. Pei, *Phys. Rev. C* **83**, 034305 (2011).
- [31] J. McDonnell, N. Schunck and W. Nazarewicz, arXiv:1301.7587 [nucl-th] (2013).
- [32] J.D. McDonnell, W. Nazarewicz and J.A. Sheikh, *Phys. Rev. C* **87**, 054327 (2013).
- [33] J. Erler, K. Langanke, H.P. Loens, G. Martínez-Pinedo and P.-G. Reinhard, *Phys. Rev. C* **85**, 025802 (2012).
- [34] H. Abusara, A.V. Afanasjev and P. Ring, *Phys. Rev. C* **82**, 044303 (2010).
- [35] H. Abusara, A.V. Afanasjev and P. Ring, *Phys. Rev. C* **85**, 024314 (2012).
- [36] B.-N. Lu, E.-G. Zhao and S.-G. Zhou, *Phys. Rev. C* **85**, 011301 (2012).
- [37] P. Ring and P. Schuck, *The Nuclear Many-Body Problem* (Springer, Berlin, 1980).
- [38] J. F. Berger, M. Girod, and D. Gogny, *Nucl. Phys. A* **428**, 23c (1984).
- [39] F. Chappert, M. Girod, and S. Hilaire, *Phys. Lett. B* **668**, 420 (2008).
- [40] S. Goriely, S. Hilaire, M. Girod and S. Péru, *Phys. Rev. Lett.* **102**, 242501 (2009).
- [41] J. Dechargé and D. Gogny, *Phys. Rev. C* **21**, 1568 (1980).
- [42] M. Baldo, L. M. Robledo, P. Schuck and X. Viñas, *Phys. Rev. C* **87**, 064305 (2013).
- [43] S. A. Giuliani, L.M. Robledo and R. Rodríguez-Guzmán, *Phys. Rev. C* **90**, 054311 (2014).
- [44] W. Nazarewicz and J. Dobaczewski, *Phys. Rev. Lett.* **68**, 154 (1992).
- [45] S. Aberg and L. -O. Jönsson, *Z. Phys. A* **349**, 205 (1994).
- [46] T. Shneidman, G. Adamian, N. Antonenko, S. Ivanova and W. Scheid, *Nucl. Phys. A* **671**, 119 (2006).
- [47] V. V. Pashkevich, *Nucl. Phys. A* **169**, 275 (1971).
- [48] P. Möller, *Nucl. Phys. A* **192**, 529 (1972).
- [49] S. Ćwiok, W. Nazarewicz, J. Saladin, W. Plóciennik and A. Johnson, *Phys. Lett. B* **322**, 304 (1994).
- [50] R. Bengtsson, I. Ragnarsson, S. Aberg, A. Gyurkovich, A. Sobczewski and K. Pomorski, *Nucl. Phys. A* **473**, 77 (1987).
- [51] K. Rutz, J. Mahrn, P. -G. Reinhard and W. Greiner, *Nucl. Phys. A* **590**, 680 (1995).
- [52] J. F. Berger, M. Girod, and D. Gogny, *Nucl. Phys. A* **502**, 85 (1989).
- [53] J. Zhao, B. -N. Lu, D. Vretenar, E. -G. Zhao, S. -G. Zhou, *Phys. Rev. C* **91**, 014321 (2015).
- [54] R. Rodríguez-Guzmán, L.M. Robledo and P. Sarriguren, *Phys. Rev. C* **86**, 034336 (2012).
- [55] L.M. Robledo and R. Rodríguez-Guzmán, *J. Phys. G: Nucl. Part. Phys.* **39**, 105103 (2012).
- [56] A. Baran, K. Pomorski, A. Lukasiak and A. Sobczewski, *Nucl. Phys. A* **361**, 83 (1981).
- [57] N. Dubray and D. Regnier, *Comput. Phys. Commun.* **183**, 2035 (2012).
- [58] L.M. Robledo and G. F. Berstch, *Phys. Rev. C* **84**, 014312 (2011).
- [59] A. Baran, *Phys. Lett. B* **76**, 8 (1978).
- [60] A. Baran, J. A. Sheikh, J. Dobaczewski, W. Nazarewicz and A. Staszczak, *Phys. Rev. C* **84**, 054321 (2011).
- [61] M. Girod and B. Grammaticos, *Nucl. Phys. A* **330**, 40 (1979).

- [62] M.J. Giannoni and P. Quentin, Phys. Rev. C **21**, 2060 (1980).
- [63] M.J. Giannoni and P. Quentin, Phys. Rev. C **21**, 2076 (1980).
- [64] J. Libert, M. Girod and J.P. Delaroche, Phys. Rev. C **60**, 054301 (1999).
- [65] R. Rodríguez-Guzmán, J.L. Egido and L.M. Robledo, Phys. Lett. B **474**, 15 (2000); Phys. Rev. C **62**, 054319 (2000).
- [66] J.L. Egido and L.M. Robledo, Lectures Notes in Physics **641**, 269 (2004).
- [67] M. Brack, J. Damgaard, A.S. Jensen, H.C. Pauli, V.M. Strutinsky and C.Y. Wong, Rev. Mod. Phys. **44**, 320 (1972).
- [68] S. Hilaire and M. Girod, Eur. Phys. J. A **33**, 237 (2007).
- [69] R. Rodríguez-Guzmán, L.M. Robledo and M. M. Sharma, Eur. Phys. J. A **51**, 73 (2015).
- [70] T. R. Rodríguez, A. Arzhanov and G. Martínez-Pinedo, Phys. Rev. C **91**, 044315 (2015).
- [71] J.F. Berstch and H. Flocard, Phys. Rev. C **43**, 2200 (1991).
- [72] H. Goutte, J.F. Berger, P. Casoli and D. Gogny, Phys. Rev. C **71**, 024316 (2005).
- [73] N. Nenoff, P. Bringel, A. Bürger, S. Chmel, S. Dababneh, M. Heil, H. Hübel, F. Käppeler, A. Neusser-Neffgen and R. Plag, Eur. Phys. J. A **32**, 165 (2007).
- [74] M. Piessens, E. Jacobs, S. Pommé and D. D. Frenne, Nucl. Phys. A **556**, 88 (1993).
- [75] G. M. Ter-Akopian, J. H. Hamilton, Yu. Ts. Oganessian, A. V. Daniel, J. Kormicki, A. V. Ramayya, G. S. Popeko, B. R. S. Babu, Q.-H. Lu, K. Butler-Moore, W. -C. Ma, S. Cwiok, W. Nazarewicz, J. K. Deng, D. Shi, J. Kliman, M. Morhac, J. D. Cole, R. Aryaeinejad, N. R. Johnson, I. Y. Lee, F. K. McGowan and J. X. Saladin, Phys. Rev. Lett. **77**, 32 (1996).
- [76] D.C. Hoffman and M.M. Hoffman, Ann. Rev. Nucl. Sci. **24**, 151 (1974).
- [77] L. Dematté, C. Wagemans, R. Barthélémy, R. D'ont and A. Deruytter, Nucl. Phys. A **617**, 331 (1997).
- [78] B. D. Wilkins, E. P. Steinberg and R. R. Chasman, Phys. Rev. C **14**, 1832 (1976).
- [79] A. Mamdouth, J. M. Pearson, M. Rayet and F. Thounder, Nucl. Phys. A **679**, 337 (2001).
- [80] M. Bender, K. Rutz, P.-G. Reinhard, J.A. Maruhn and W. Greiner, Phys. Rev. C **58**, 2126 (1998).
- [81] K.-H. Schmidt et al., Nucl. Phys. A **665**, 221 (2000).
- [82] J. Sadhukhan, K. Mazurek, A. Baran, J. Dobaczewski, W. Nazarewicz and J. A. Sheikh, Phys. Rev. C **88**, 064314 (2013).
- [83] F. Lechaftois, I. Deloncle and S. Péru, Phys. Rev. C **92**, 034315 (2015).
- [84] S. Perez-Martin and L.M. Robledo, Phys. Rev. C **78**, 014304 (2008).
- [85] R. Rodríguez-Guzmán, P. Sarriguren, L.M. Robledo and S. Perez-Martin, Phys. Lett. B **691**, 202 (2010).
- [86] R. Rodríguez-Guzmán, P. Sarriguren and L.M. Robledo, Phys. Rev. C **82**, 044318 (2010); Phys. Rev. C **82**, 061302 (2010); Phys. Rev. C **83**, 044307 (2011).